

Article

Effect of Aeration on the Cavitation Characteristics of the Control Valve in Hydro-Driven Ship Lifts

Jiao Wang ^{1,2} , Yaan Hu ³, Liang Chen ², Ruichang Hu ^{1,2} and Hao Yuan ^{1,2,*}

¹ Southwest Water Conservancy and Water Transport Engineering Research Institute, Chongqing Jiaotong University, Chongqing 400010, China; jwang@cqjtu.edu.cn (J.W.)

² Chongqing Xike Consultation for Water Transport Co., Ltd., Chongqing 400074, China

³ Key Laboratory of Navigation Structures State, Key Laboratory of Hydrology-Water Resources and Hydraulic Engineering, Nanjing Hydraulic Research Institute, Nanjing 210029, China

* Correspondence: yuanhao@cqjtu.edu.cn

Abstract: In hydro-driven ship lifts, plunger valves and fixed cone valves are the most suitable structures for achieving accurate flow control under a wide range of flow conditions. In order to inhibit cavitation in these valve structures, experiments were conducted in which forced aeration was applied before the valve. The cavitation phenomena and aerated flow regime were observed through a transparent glass pipe, and the cavitation noise characteristics were recorded using a hydrophone. The test results show that aeration can reduce the valve working cavitation number, albeit to a limited degree (<5%). Based on the sound velocity theory of aerated flow and the experimental results, the relationship between the aeration concentration and the cavitation inhibition efficiency was obtained. When the aeration concentration is approximately 0.1%, cavitation can be significantly inhibited via forced aeration before the valve. Once the aeration concentration reaches 0.9%, the cavitation inhibition efficiency becomes saturated. The research results presented in this paper provide a reference for the cavitation inhibition of industrial valves.

Keywords: aeration concentration; wall pressure; cavitation number; cavitation noise; ship lift



Citation: Wang, J.; Hu, Y.; Chen, L.; Hu, R.; Yuan, H. Effect of Aeration on the Cavitation Characteristics of the Control Valve in Hydro-Driven Ship Lifts. *Water* **2023**, *15*, 4014. <https://doi.org/10.3390/w15224014>

Academic Editor: Giuseppe Pezzinga

Received: 26 October 2023

Revised: 11 November 2023

Accepted: 14 November 2023

Published: 19 November 2023



Copyright: © 2023 by the authors. Licensee MDPI, Basel, Switzerland. This article is an open access article distributed under the terms and conditions of the Creative Commons Attribution (CC BY) license (<https://creativecommons.org/licenses/by/4.0/>).

1. Introduction

The Yangtze River Golden Channel is the most important inland waterway in China, significantly contributing to the social and economic development of cities along the Yangtze River. In recent decades, inland navigation channels (such as the Yangtze River) have developed rapidly. On the one hand, these navigation channels have undergone large-scale restoration and construction, and their level and navigation capacity have significantly improved. On the other hand, important water conservancy projects (such as the Three Gorges Dam) are equipped with large-capacity ship lifts, which satisfy the demands of large ships passing through high dams. With the new demand for green development in rivers, the construction of ecological waterways has begun and achieved good results. Vegetation-based restoration methods (e.g., planting aquatic vegetation [1,2]) have been employed to protect floodplains and central bars from bed erosion, increasing the riverbed stability of navigation channels. For example, Liu and Shan [3] systematically studied the impact of vegetation on flow evolution and sediment transport, providing guidance for vegetation-based ecological restoration projects in navigation channels. At the same time, with the rapid development of inland shipping, the cargo capacity of ships gradually increases, corresponding to the increasing load requirements for ship lifts. This paper focuses on ship lifts, and the main goal of our study was to examine the impact of aeration on the cavitation characteristics of control valves in the lifts, which ensure the safe operation of ship lifts.

The Jinghong ship lift is the first HDSL in the world (Figure 1), with a maximum lifting height of 66.86 m. The core component of this HDSL is the control valve, which is

similar to the electric motor in an electric-driven ship lift and is the key to the safe and efficient operation of the ship lift [4]. Thus, a high-performance control valve is required to control the flow rate accurately, with the potential to accommodate significant changes in flow conditions. At present, only plunger valves and fixed cone valves satisfy these requirements [5]. Under high pressure differences, it is difficult to avoid cavitation in the control valve. Controlling the cavitation damage in the valve and pipeline is the key to the safe and efficient operation of HDSLs [6].

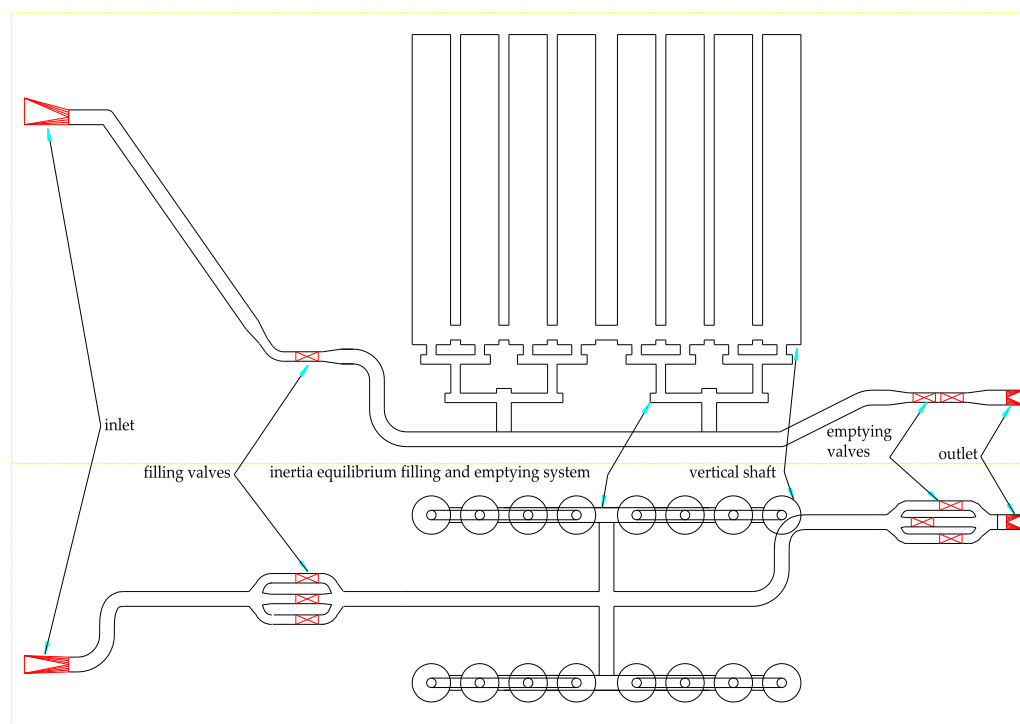


Figure 1. A schematic drawing of the Jinghong HDSL.

Research on cavitation in industrial valves has mainly focused on the influence of the valve geometry [7–9] and valve operation mode [10]. Chern [11] studied a globe valve with and without a cage using a cavitation model and showed that the cage could limit the cavitation in the vicinity of the cage and prevent the cavitation from eroding the valve body and downstream pipe. Jo [12] conducted a numerical study on reducing cavitation in a butterfly valve and found that a perforated plate was effective in suppressing the cavitation inside the pipe. Lee [13] designed the bottom plug used in three-way reversing valves to minimize the cavitation effect, while Han [14] tested three typical designs for poppet valves. The results revealed that a two-stage throttle valve can effectively suppress the occurrence of cavitation, although the flow force of this valve type is much higher than for other valves. The optimization of the valve structure could effectively improve the anti-cavitation performance of the valve, but the universality of current designs is poor.

In addition to optimizing the valve structure, aeration is another effective means of preventing cavitation. The most important factor affecting aeration is the aeration concentration. Many researchers have suggested that cavitation erosion can be significantly mitigated when the air concentration near a wall is 1–2% and may be eliminated when the air concentration reaches 5–7% [15]. The aeration concentration at which cavitation is inhibited depends on the specimen materials. Rasmussen [16] suggested an aeration rate of 1% to avoid the cavitation erosion of an aluminum alloy specimen, while Russell and Sheehan [17] reported that an air concentration of 5.7% was suitable for a concrete specimen. The pressure in the cavitation region of a high-velocity flow with aeration increases because of the formation of a compression wave after the flow has been aerated [18]. Theoretical analysis has determined the relationship between the aeration concentration (C) and the

acoustic velocity of sound in water (v_a) [19]. The air bubble size also affects the degree of cavitation inhibition [20–22]. Smaller bubbles are more conducive to inhibiting cavitation erosion, whereas bigger bubbles float and break more easily, which reduces the aeration concentration on side walls [23]. Small air bubbles tend to alleviate cavitation erosion, even at the same air concentration [24]. Li made the prediction of aeration from data-driven and multi-gene genetic programming methods [25,26]. These studies have had a strong guiding effect on the design of experimental models.

The aeration mode can be determined as either self-aeration or forced aeration. Self-aeration uses negative pressure to achieve natural aeration [27,28], such as in spillway aeration [29] and lock water valve aeration [30,31]. Forced aeration requires an air compressor to achieve passive aeration. Self-aeration methods are relatively simple but cannot suppress the primary cavitation inside a valve. Forced aeration protects the pipeline after the valve, inhibits cavitation initiation, and protects the internal valve structure.

In conclusion, existing studies related to reducing cavitation erosion via aeration have mainly focused on microscopic aspects [32,33] and self-aeration [34]. There have been few studies on macroscopic engineering applications and forced aeration. The specific effects of forced aeration on cavitation inhibition remain unclear. Studies have shown that forced aeration is necessary to protect the control valves in HDSLs [35], but large-scale aeration is not conducive to the stability of the shaft water surface. Thus, it is necessary to study the reasonable aeration concentration that can be achieved by forced aeration. In this study, forced aeration tests were conducted for the two types of industrial valves suitable for HDSLs. The cavitation characteristics in the valve segments at different opening degrees, flow rates, and aeration concentrations were studied. The structure of the flow field and the cavitation phenomenon were observed via high-speed photography [36–38]. Analyses of the influence of aeration on the cavitation number and the relationship between the aeration concentration and cavitation inhibition efficiency are presented in this paper to provide a reference for similar engineering projects.

2. Experimental Setup

The experiments were carried out in the multi-functional cavitation experiment hall of Nanjing Hydraulic Research Institute, China. This laboratory offers automated control of pumps, valves, and pressure and flow monitoring (Figure 2). The maximum capacity of the water pressure supply system was 1.5 MPa and the maximum flow rate was 0.15 m³/s. The experimental model combined a flow control system, aeration equipment, a test valve, a glass pipe, and a data acquisition system. As seen in Figure 3, there were two types of test valves: a plunger valve with an SZ 20–30% sleeve and a cone valve with a dome. The diameter of the test valves was 150 mm. The sensor layout and aeration ring design are shown in Figure 4. Based on recent research [39], we adopted a smaller, air-filled hole for aeration: the hole's diameter was 3 mm, and the number of holes was 32. The aeration concentration range was set to 0–4%. The sensor characteristics are listed in Table 1.

The aeration concentration (C) of each test is listed in Table 2. The maximum aeration concentration was about 4%. The aeration concentration is defined as:

$$C = \frac{Q_a}{Q_a + Q_w} \quad (1)$$

where Q_a is the air flow (m³/h) and Q_w is the water flow (m³/h).

The typical experimental process involves adjusting the valve to the test opening degree, stabilizing the downstream pressure (P_d) at 60/120/180 kPa (P_d in Table 2 is 180 kPa because the test results fluctuate less under a higher P_d), and then gradually increasing the upstream pressure (P_u) until primary cavitation occurs in the valve. The upstream and downstream control pressures need to be adjusted repeatedly. The criteria for identifying the primary cavitation state (σ_i) of the valve include intermittent pulses of cavitation noise, a sizzling sound inside the valve, and tiny visible cavitation bubbles in the water flow. Based on the primary cavitation state, P_u was calculated according to the

relative cavitation number $\sigma/\sigma_i = 0.4$ (strong cavitation state), and then the upstream stable pressure was adjusted to this value. Once the flow field structure was stable, the cavitation noise and flow field structure were measured. Finally, forced aeration tests were conducted under different air flow rates ($Q_a = 0.1\text{--}3\text{ m}^3/\text{h}$), and the cavitation noise and flow field structure were repeatedly measured. The experiments were repeated at least three times, and experimental error was reduced by taking the mean value of multiple experimental results. The cavitation inhibition effect of forced aeration was explored by analyzing the flow field structure, cavitation number, and noise characteristics. The cavitation number σ is defined as [3]:

$$\sigma = \frac{P_d/(\rho g) + (P_{atm} - P_{sv})/(\rho g)}{(P_u - P_d)/(\rho g) + v^2/2g} \tag{2}$$

where P_{atm} is the local atmospheric pressure; P_{sv} is the local saturated vapor pressure; v is the average velocity in the reference section; P_u is the upstream steady pressure; and P_d is the downstream steady pressure.

1 pump; 2 control valve; 3 bypass valve; 4 electromagnetic flowmeter; 5 pressure stabilizing box; 6 electronic pressure gauge; 7 aeration ring; 8 test valve; 9 glass tube; 10 air flow meter; 11 air compressor; 12 hydrophone; 13 pressure sensor; 14 data acquisition system; 15 computer; 16 camera; 17 pool

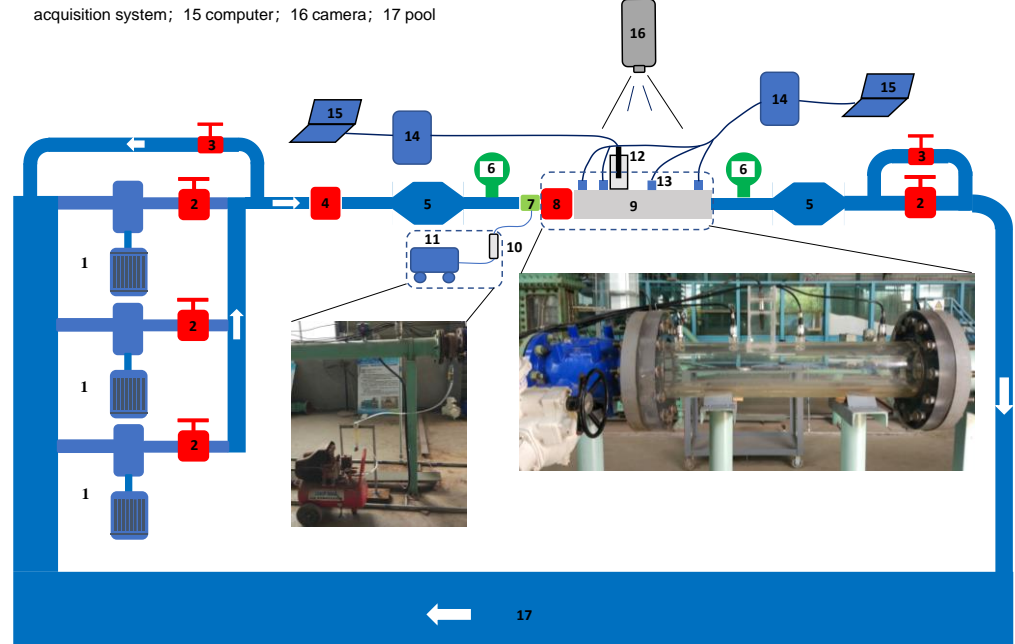


Figure 2. Experimental setup.



Figure 3. Test valves: (a) fixed cone valve; (b) plunger valve.

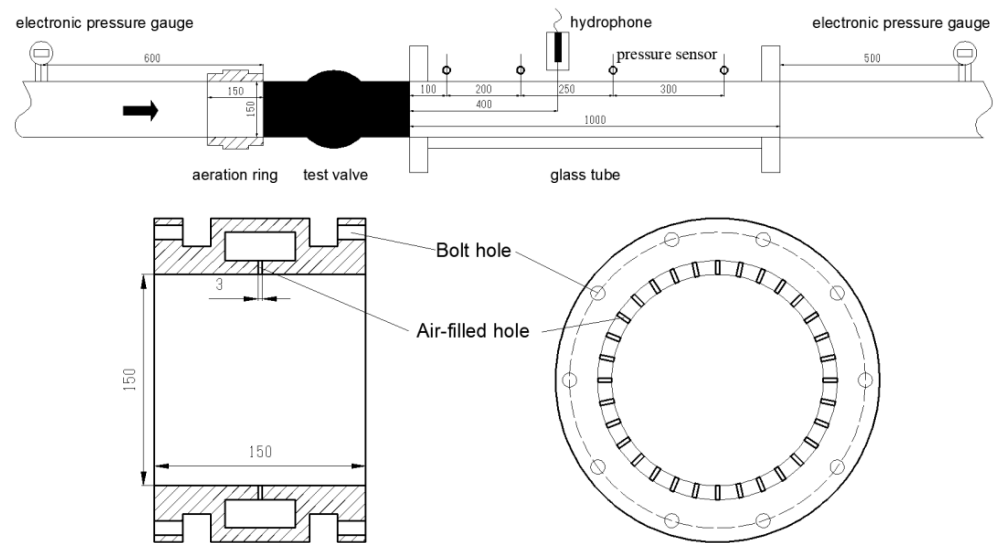


Figure 4. Sensor layout and aeration ring design (units: mm).

Table 1. Sensor characteristics.

Equipment	Parameter	Value	Physical Quantity	Model
Electromagnetic flowmeter	Range	0–15 m/s	Q_w	E—mag E
	Accuracy	±0.3% of the indicated value (flow velocity ≥ 1 m/s); ±3 mm/s (flow velocity < 1 m/s)		
Hydrophone	Effective frequency	3–300 kHz	SPL	RHSA-10
	Accuracy	±1 dB		
Pressure sensor	Range	0–1 MPa	Wall pressure	HQ130
	Accuracy	±0.0001 MPa		
Air flow meter	Range	0–3 m ³ /h	Q_a	GL10-15B
	Accuracy	±0.05 m ³ /h		
Electronic pressure gauge	Range	0–4 MPa	P_u, P_d	YPR-YBS-C
	Accuracy	±0.001 MPa		
Camera	Maximum field of view	700 mm × 700 mm	Flow field structure	Phantom
	Maximum resolution	3840 × 2160		

Table 2. Experimental conditions.

Valve Type	Valve Opening (n)	Average Flow Velocity (m/s)	Q_a (m ³ /h)						
			0	0.1	0.3	0.6	1.2	2	3
Plunger valve	0.3	1.152	0	0.14	0.41	0.82	1.64	2.74	4.08
	0.5	1.689	0	0.09	0.28	0.56	1.13	1.87	2.79
	0.6	3.840	0	0.04	0.12	0.25	0.49	0.82	1.23
	0.9	5.666	0	0.03	0.08	0.17	0.33	0.56	0.83
Cone valve	0.1	1.302	0	0.12	0.36	0.73	1.46	2.42	3.63
	0.2	3.149	0	0.05	0.15	0.30	0.60	1.00	1.50
	0.3	4.932	0	0.03	0.10	0.19	0.38	0.64	0.96

3. Results and Analysis

3.1. Flow Coefficient

The variation in the flow coefficient with respect to the aeration concentration is shown in Figure 5. At different flow rates, the flow coefficient decreases with increasing aeration concentration, but the rate of decrease becomes slower. Under the same aeration concentration, a larger flow velocity produces a more obvious drop in the flow coefficient. From its definition, the flow coefficient is proportional to the flow rate and inversely proportional to the pressure difference. The test results show that the forced air intake in front of the valve produces a certain resistance to the incoming flow. This enforces a reduction in the flow rate over the valve, which enhances the pressure in front of the valve. The pressure behind the valve also increases, but to a lesser degree than that before the valve. Thus, the pressure difference continues to increase, and the flow coefficient continues to decline. With an increase in air content, the flow coefficient decreases continuously. This is because the pressure in front of the valve does not increase simultaneously with the increase in air content, and so the flow coefficient exhibits a relative decrease. Under the test conditions considered in this study, the maximum air content was 3 m³/h, the flow rate v ranged from 1.152 to 5.666 m/s, and the air content C varied from 0% to 4%. The maximum reduction in the flow coefficient was less than 5%, indicating that the air content has little effect on the flow coefficient.

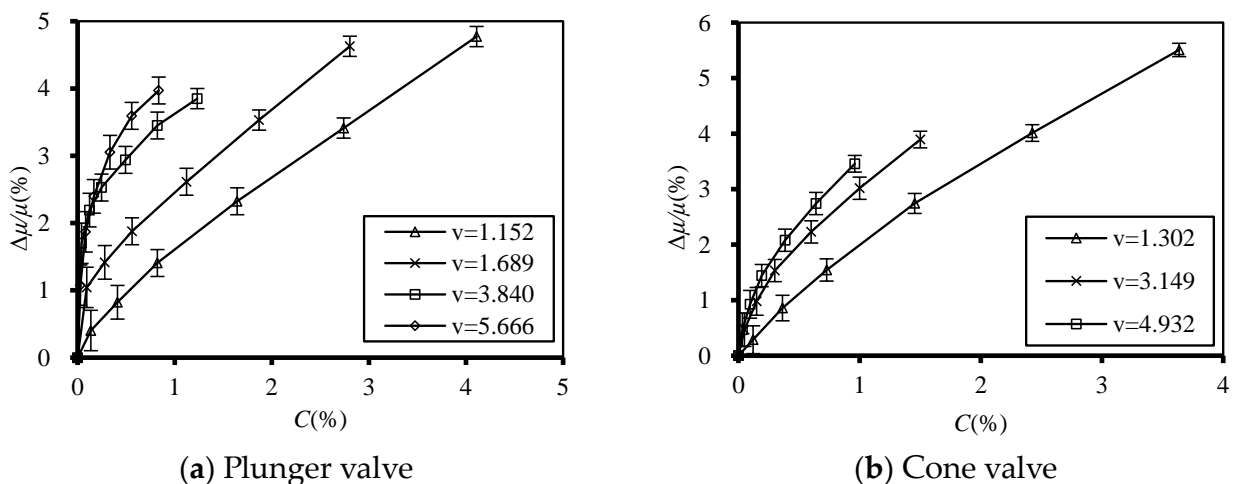


Figure 5. Variation in flow coefficient with aeration concentration.

3.2. Wall Pressure

The variations in the pressure characteristics under different working conditions at measuring point one (100 mm away from the valve port) with respect to the aeration concentration are shown in Figure 6. By comparing the dimensionless time-averaged pressure (P_{av}) on the pipe wall under different working conditions, it can be seen that little change occurs as the aeration concentration increases. In contrast, the dimensionless tube wall pulsation pressure (P_{rms}) exhibits an obvious dependence on the aeration concentration when the valve opening is small and the average flow rate in the section is low. As the aeration concentration increases, the pressure pulsation coefficient continues to increase, but the rate of increase gradually slows. This is because the turbulence in the flow field is weak under small-opening and low-flow-velocity conditions, and air entrainment significantly increases the turbulence of the flow. The pressure characteristics on the walls behind the two types of valves are quite different, mainly because the flow field structure behind the plunger valve is quite different under different opening degrees, and the influence of aeration on the wall pressure characteristics is more obvious. However, the flow field structure of the cone valve with different opening degrees shows little difference, and the influence of aeration on the pressure characteristics on the wall is small.

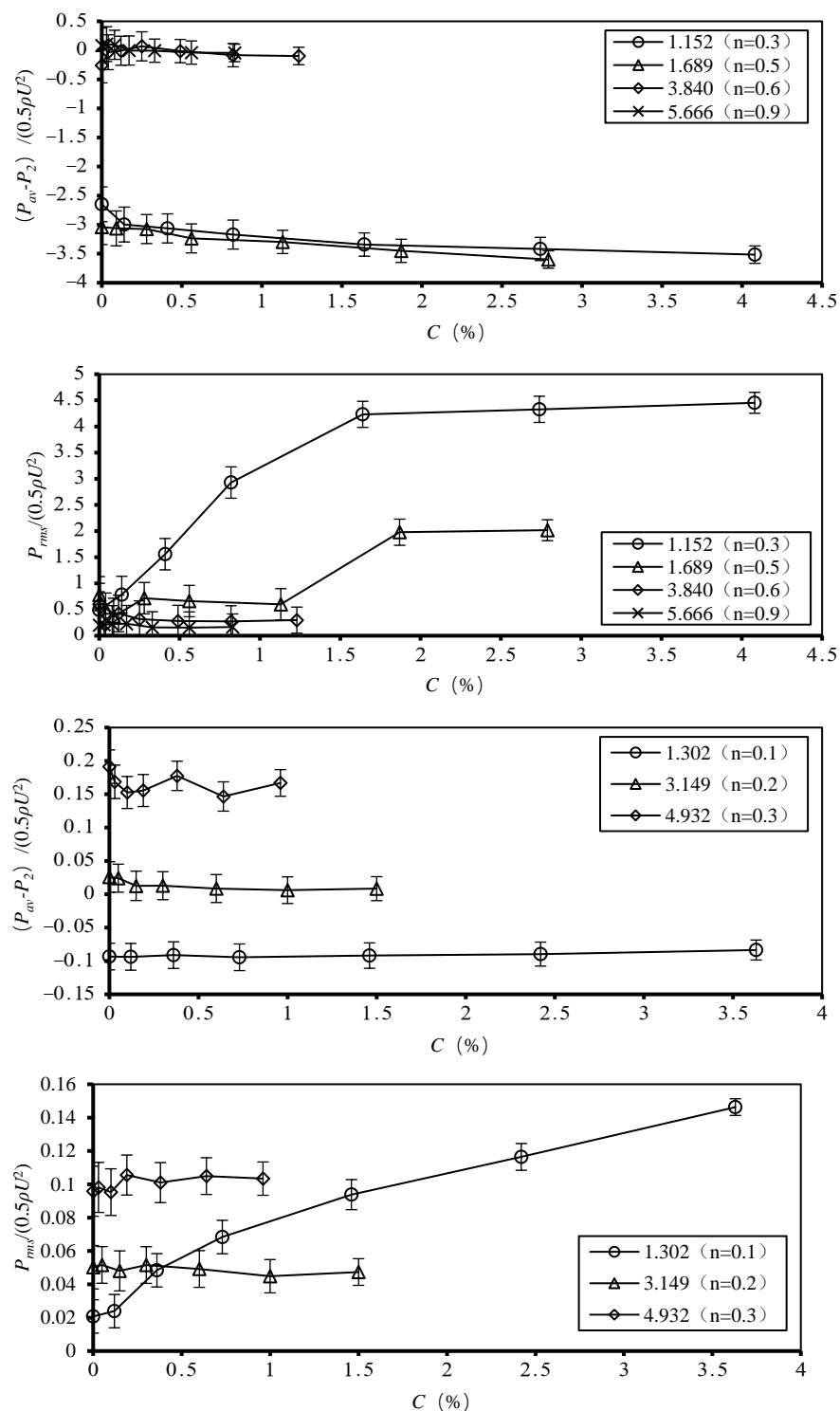


Figure 6. Variation in wall pressure with aeration concentration.

As the concentration of entrained air increases, the turbulence intensity's rate of increase in the flow field decreases. Forced aeration before the valve affects the flow field structure behind the valve and increases the turbulence intensity of the water body. For a flow field with insufficient turbulence, air entrainment obviously increases the turbulence of the flow field and has a significant influence on the wall pressure. If the flow field is sufficiently turbulent, a small amount of aeration has a negligible effect on the flow field. The wall pressure characteristics of the cone valve are consistent with those of the plunger valve, indicating that the valve type has little influence on the aeration effect.

3.3. Cavitation Phenomena

Typical post-valve cavitation phenomena are shown in Figure 7 for a valve opening degree of 0.3. The main type of cavitation across both valves is foggy cavitation. The symmetrical runner design of the plunger valve causes cavitation bubbles to converge in a spiral rope at the center of the pipe. The flow oscillates back and forth in an unstable flow field structure, and the impact on the pipe wall is strong. After the foggy cavitation gathers into a rope, the cavitation is harder to suppress. The rectification and limitation of the dome make the flow regime more uniform after the cone valve, with the cavitation bubbles evenly distributed in the flow.

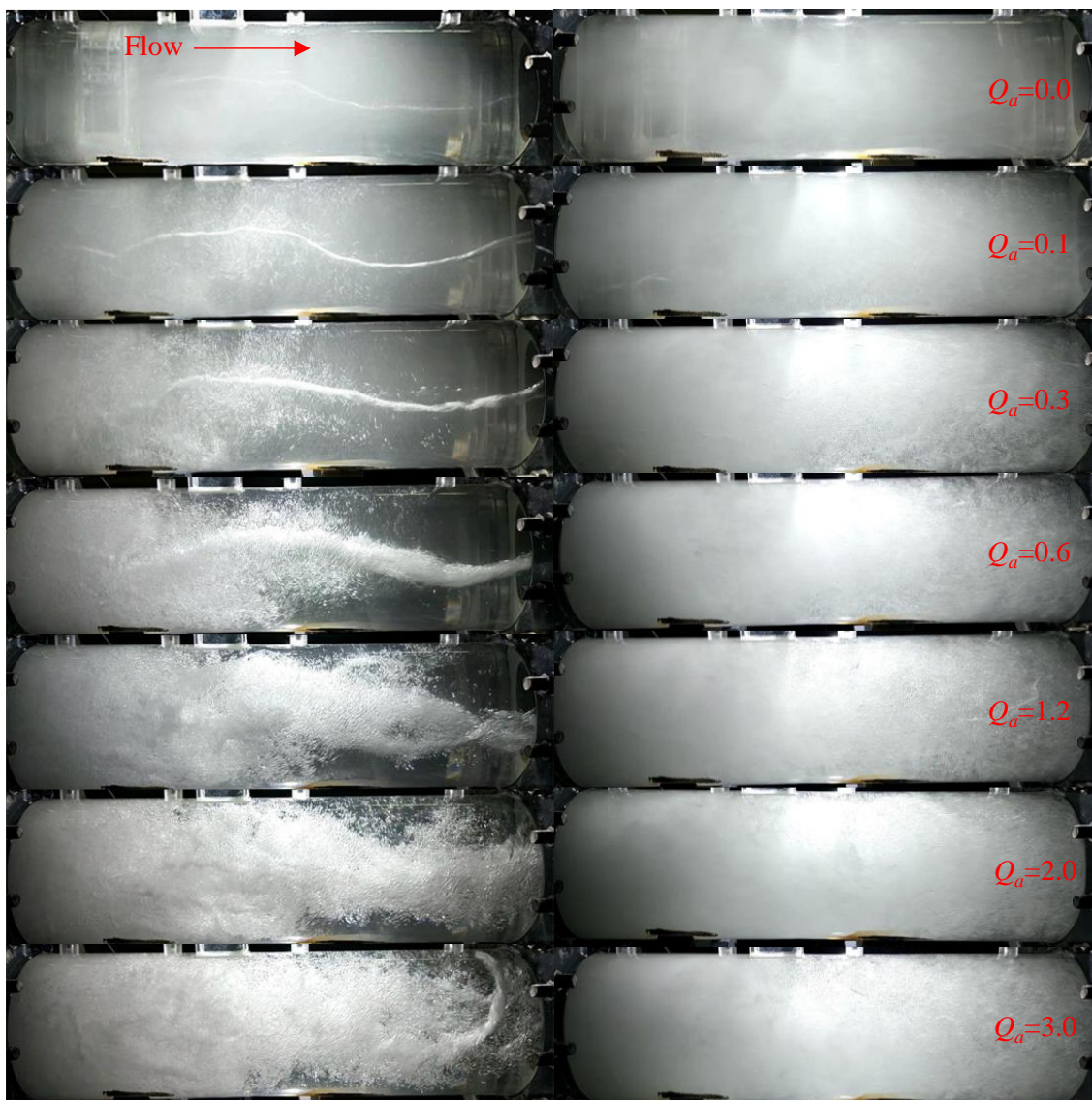


Figure 7. Cavitation phenomena (left: plunger valve; right: cone valve).

After aeration, the flow field structure behind the plunger valve is gradually destroyed. When $Q_a = 0.10 \text{ m}^3/\text{h}$ (0.1% of the mainstream), the dynamic process of small air bubbles converging into the spiral rope cavitation can be observed. The incorporation of air bubbles gradually thickens the spiral rope cavitation. However, the limitation imposed by water flow convergence leads to an increasing number of scattered air bubbles in the water flow. When $Q_a = 1.20 \text{ m}^3/\text{h}$ (1.5% of the mainstream), there are too many air bubbles in the water flow, and the multiple strands of spiral rope cavitation mix with each other, making the flow pattern very unstable.

Comparison experiments indicate that the flow field structure after the cone valve is relatively stable, with no significant changes as the level of aeration increases. With a low level of aeration, fine, needle-like air bubbles are evenly distributed in the water flow. As the air content increases, the number of air bubbles in the water flow obviously increases and the visibility of the water flow gradually decreases, but the flow field structure after the cone valve remains relatively unchanged.

3.4. Working Cavitation Number

The variation in the working cavitation number under test conditions with respect to the aeration concentration is shown in Figure 8 ($\Delta\sigma = \sigma_a - \sigma$, where σ_a is the cavitation number with aeration). Forced aeration has a certain blocking effect on the flow before the valve, resulting in a decrease in the valve overflow capacity. Increasing the aeration concentration enhances both P_u and P_d , although the former grows faster than the latter, so the working cavitation number decreases. Under the experimental conditions in this study, the maximum air content was 3 m³/h, the flow velocity ranged from 1.152 to 5.666 m/s, and the air concentration range was 0–4%. The maximum reduction in the working cavitation number was less than 5%, which indicates that the air content has little influence on the working cavitation number.

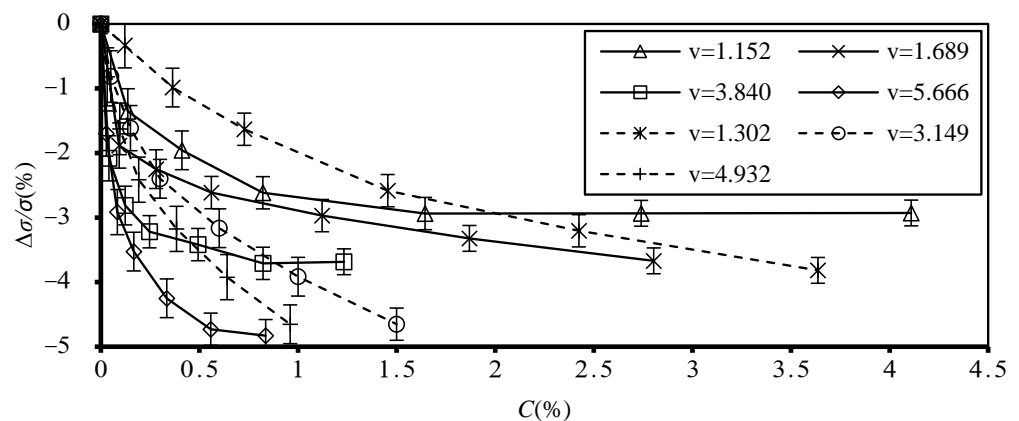


Figure 8. Variation in $\Delta\sigma/\sigma$ with C .

3.5. Cavitation Noise Characteristics

The cavitation noise collected during the tests reflects certain time domain characteristics. As this study focused on the constant cavitation characteristics, the time domain signal of cavitation noise was converted into a frequency domain signal using a Fourier transform. All complex waveforms can be regarded as the synthesis of several sine waves, and any periodic function can be formed by the superposition of multiple sine waves with different amplitudes and phases. Thus, the collected noise signal can be represented as:

$$f(t) = \sum_{i=1}^{\infty} A_i \sin[\omega_i(t) + \varphi_i(t)] \tag{3}$$

where ω_i is the frequency of the test signal, φ_i is the initial phase angle of the test signal, and $i = 1, 2, 3, \dots, n$.

The following Fourier transform was applied to convert the cavitation noise time domain features into frequency domain features:

$$F(\omega) = F[f(t)] = \int_{-\infty}^{\infty} f(t)e^{-i\omega t} dt \tag{4}$$

Cavitation noise is an important index in determining the strength of cavitation. The main characteristic parameters of cavitation noise include the noise sound pressure (SP) and the noise sound pressure level (SPL), which are related according to:

$$SPL = 20\lg\left(\frac{SP}{P_r}\right) \tag{5}$$

where P_r is the reference sound pressure, usually taken as 2×10^{-5} Pa.

The variation in SPL under typical test conditions with different aeration concentrations is shown in Figure 9. The SPL value is very high in the frequency domain without aeration. When a small amount of air is added, the SPL value decreases rapidly. With a further increase in the air concentration, the downward trend of SPL obviously slows down, and finally drops to the background noise level of the water flow. The dominant frequency of the SPL is about 6 kHz. The maximum SPL (SPL_{max}) in the dominant frequency under different aeration concentrations is shown in Figure 10.

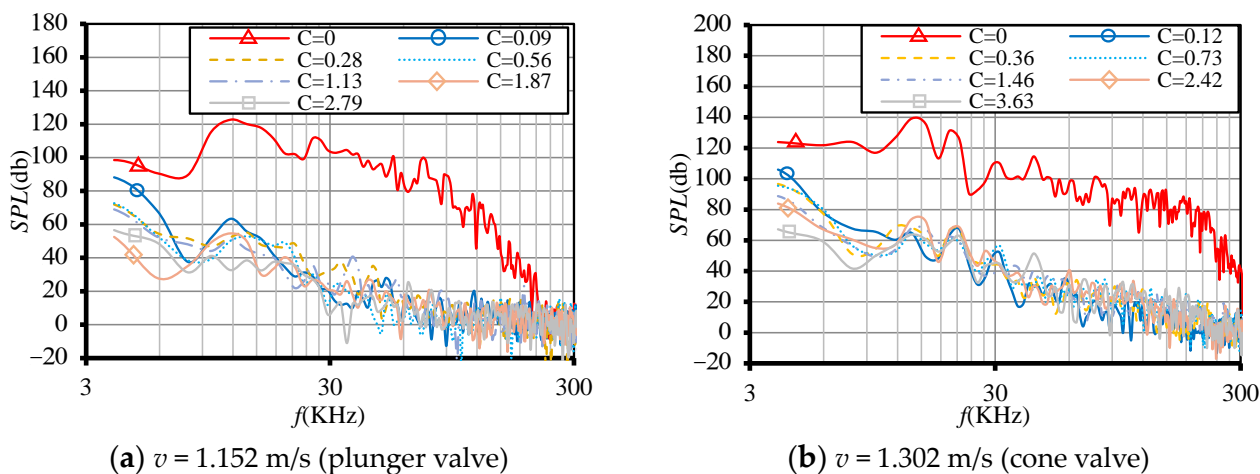


Figure 9. SPL under different aeration concentrations.

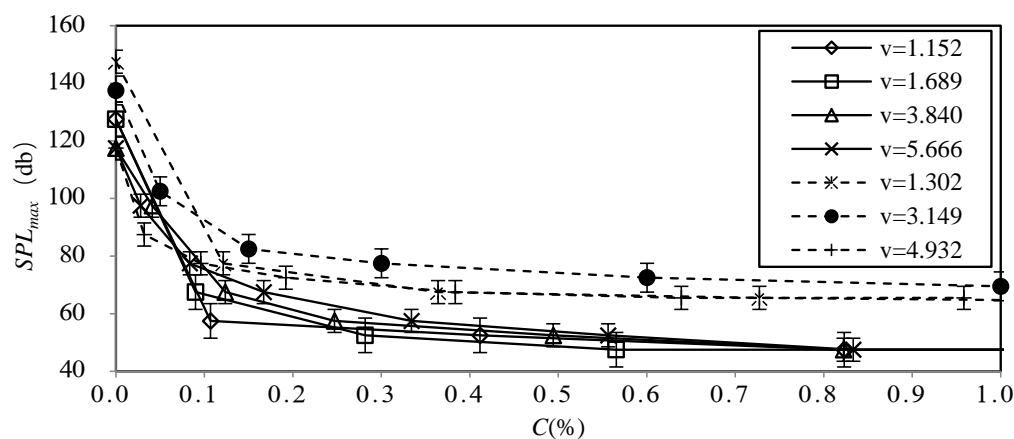


Figure 10. SPL_{max} under different aeration concentrations.

Figure 10 shows that the variations in SPL_{max} with aeration are similar at different velocities. When $C \approx 0.1\%$, SPL_{max} drops rapidly by more than 60%; with increasing aeration concentration, the rate of decline in SPL_{max} is significantly reduced. When $C \approx 0.9\%$, SPL_{max} has dropped to a stable value and remains largely unchanged with further increases in the aeration concentration. This indicates that, when $C \approx 0.1\%$, cavitation can be significantly inhibited, and when $C \approx 0.9\%$, the cavitation inhibition effect induced by forced aeration has become saturated.

Aeration changes the propagation velocity of sound waves in water flow [18]. The theoretical relationship between the acoustic velocity of aerated flow and the aeration concentration is presented in Equation (6). Figure 11 shows the theoretical curve of acoustic velocity with respect to the aeration concentration in the plunger valve. The acoustic velocity decreases rapidly with increasing aeration concentration, and the trend is very similar to that of SPL_{max} in the dominant frequency. This indicates that reducing cavitation using forced aeration is closely related to the decrease in the acoustic velocity.

$$v_a \approx \sqrt{\frac{p}{\rho_w C(1 - C)}} \tag{6}$$

where v_a is the acoustic velocity of sound in water, and ρ_w is the density of water.

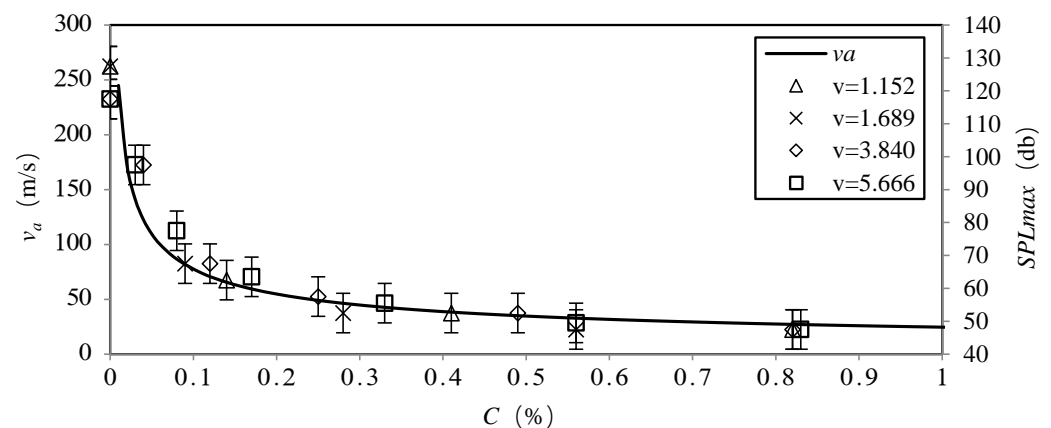


Figure 11. Comparison of theoretical acoustic velocity and SPL_{max} in the dominant frequency.

Based on the comparison of theoretical acoustic velocity and SPL_{max} in the dominant frequency, the cavitation inhibition efficiency η is defined as follows:

$$\eta = \frac{SPL_{max} - SPL_a}{SPL_{max} - SPL_{amin}} \tag{7}$$

where η is the cavitation inhibition efficiency; SPL_{max} is the maximum sound pressure level in the dominant frequency without aeration; SPL_a is the sound pressure level in the dominant frequency with aeration; and SPL_{amin} is the minimum sound pressure level in the dominant frequency with aeration.

Based on the test results obtained in this study, the empirical formula relating the cavitation inhibition efficiency by aeration and the aeration concentration is presented in Equation (8). As the cavitation inhibition efficiency is not only affected by acoustic velocity, a correction factor of $m = 1.08$ is introduced.

$$\eta = m(1 - \frac{0.009}{\sqrt{C(1 - C)}}) \tag{8}$$

A fitting curve based on Equation (8) is compared with the experimental values in Figure 12. The cavitation noise in both valves is significantly suppressed by aeration. Under the same aeration concentration, η is higher in the cone valve than the plunger valve for $C < 0.3\%$, which indicates that a small amount of aeration produces a more obvious inhibition effect on cavitation in the cone valve. When $C > 0.3\%$, this effect is no longer obvious. Because the flow regime after the plunger valve is complex, cavitation bubbles may form a slender region of spiral cavitation, which reduces the effect of aeration. Hence, the cavitation inhibition efficiency of aeration in the plunger valve is lower. Larger values of Q_a damage the flow field structure after the plunger valve, which enhances the mixing

effect of cavitation bubbles and air bubbles. Therefore, the difference in the corrosion reduction effects of aeration between the two types of valves is reduced.

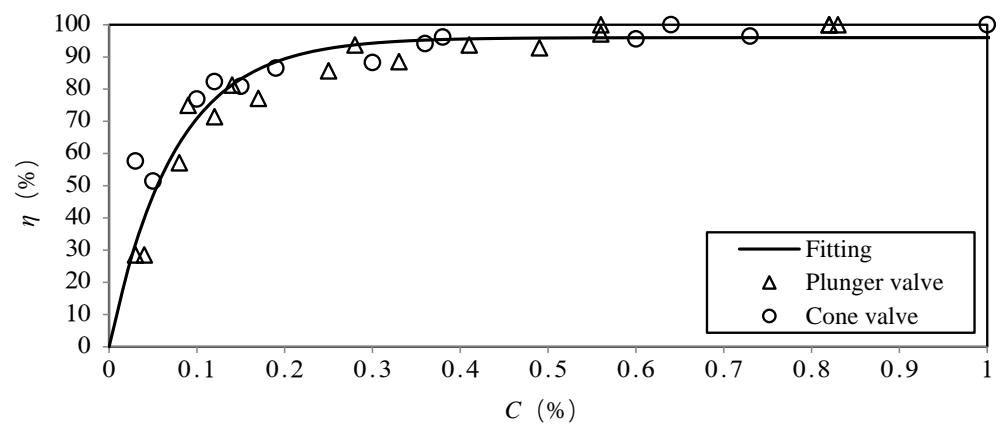


Figure 12. Fitting relationship of η and C .

In summary, from a macroscopic view, the flow field structure of the two types of valves is quite different, and a small amount of aeration has little impact on the flow field structure, while a large amount of aeration may destroy the flow field structure. From a microscopic view, a small amount of aeration can significantly inhibit valve cavitation, but a large amount of aeration cannot further improve the cavitation inhibition effect.

4. Conclusions

The working conditions of the control valve in HDSLs are very difficult, and valve cavitation is inevitable. To ensure the safety of the valve and pipeline, this study conducted forced aeration tests on two types of industrial valves that are suitable for the operational requirements of HDSLs. The main conclusions are as follows:

- (1) The test results show that forced aeration in front of the valve produces a certain resistance to the incoming flow, resulting in flow reduction. The aeration concentration in this study was less than 4%, and the reduction in the flow coefficient was less than 5%, indicating that aeration has little effect on the flow coefficient.
- (2) In flow fields with insufficient turbulence, aeration obviously increases the level of turbulence, which has a significant influence on the wall pressure. If the turbulence in the flow field is sufficiently strong, a small amount of aeration has a negligible effect on the flow field.
- (3) The main cavitation type across both valves was foggy cavitation. The flow regime after the plunger valve is complex, and cavitation bubbles may form a slender region of spiral cavitation. The flow field structure after the cone valve is simpler, with a stable, uniform flow regime containing evenly distributed cavitation bubbles that are easier to suppress.
- (4) Aeration reduces the working cavitation number, but its influence is limited. In this study, the reduction in the valve working cavitation number was less than 5%.
- (5) Aeration can significantly inhibit valve cavitation. The test results show that when $C \approx 0.1\%$, the cavitation can be significantly inhibited. When $C \approx 0.9\%$, the suppression of valve cavitation by forced aeration before the valve becomes saturated. An empirical formula relating the cavitation inhibition efficiency and the aeration concentration was obtained.

This research was based on the constant flow test condition. Valve opening and closing is an unsteady process, and the rule of aeration in this dynamic process needs to be studied further.

Author Contributions: Conceptualization, J.W. and Y.H.; methodology, L.C.; software, J.W. and R.H.; validation, J.W., Y.H. and H.Y.; formal analysis, Y.H.; investigation, L.C.; resources, H.Y.; data curation, L.C.; writing—original draft preparation, J.W.; writing—review and editing, R.H. and Y.H.; visualization, H.Y.; supervision, L.C.; project administration, J.W.; funding acquisition, H.Y. All authors have read and agreed to the published version of the manuscript.

Funding: This research was funded by the Science and Technology Research Project of Chongqing Municipality Education Commission of China (Grants No. KJQN202000722), the National Natural Science Foundation of China (Grant No. 52109076), and the Nature Science Foundation of Chongqing City (Grant No. cstc2021jcyj-msxmX1175).

Data Availability Statement: Data supporting the findings of this study are available from the authors on request.

Conflicts of Interest: Author Liang Chen was employed by the company Chongqing Xike Consultation for Water Transport Co., Ltd. The remaining authors declare that the research was conducted in the absence of any commercial or financial relationships that could be construed as a potential conflict of interest.

References

1. Shan, Y.Q.; Yan, C.H.; Liu, J.T.; Liu, C. Predicting velocity and turbulent kinetic energy inside an emergent Phragmites australis canopy with real morphology. *Environ. Fluid Mech.* **2023**, *23*, 943–963. [\[CrossRef\]](#)
2. Hu, R.C.; Zhang, J.M. Modeling velocity in a compound channel with co-existing emergent and submerged vegetation. *Phys. Fluids* **2022**, *34*, 105127. [\[CrossRef\]](#)
3. Liu, C.; Shan, Y.Q. Impact of an emergent model vegetation patch on flow adjustment and velocity. *Proc. Inst. Civ. Eng.-Water Manag.* **2022**, *175*, 55–66. [\[CrossRef\]](#)
4. Li, Z.H.; Hu, Y.A. Design theory of hydro-floating ship lift. *Port Waterw. Eng. Chin.* **2010**, *34*, 116–120. [\[CrossRef\]](#)
5. Wang, J.; Hu, Y.A.; Li, Z.H. Selection feasibility study of hydro-floating ship lift valve. *Port Waterw. Eng. Chin.* **2017**, *9*, 19–25. [\[CrossRef\]](#)
6. Xue, S. Hydraulics of Hundred-Meter Scale Hydro-Floating Ship Lift. Ph.D. Thesis, Hohai University, Nanjing, China, 2017.
7. Gholami, H.; Yaghoubi, H.; Alizadeh, M. Numerical analysis of cavitation phenomenon in a vaned ring-type needle valve. *J. Energy Eng.* **2015**, *141*, 04014053. [\[CrossRef\]](#)
8. Jin, Z.J.; Gao, Z.X.; Qian, J.Y.; Wu, Z.; Sunden, B. A Parametric Study of Hydrodynamic Cavitation Inside Globe Valves. *J. Fluids Eng.-Trans. ASME* **2018**, *140*, 031208. [\[CrossRef\]](#)
9. Jin, Z.J.; Qiu, C.; Jiang, C.H.; Wu, J.-Y.; Qian, J.-Y. Effect of valve core shapes on cavitation flow through a sleeve regulating valve. *J. Zhejiang Univ.-Sci. A* **2020**, *21*, 1–14. [\[CrossRef\]](#)
10. Qiu, C.; Jiang, C.H.; Zhang, H.; Wu, J.-Y.; Jin, Z.-J. Pressure Drop and Cavitation Analysis on Sleeve Regulating Valve. *Processes* **2019**, *7*, 829. [\[CrossRef\]](#)
11. Chern, M.J.; Wang, C.C. Control of volumetric flow-rate of ball valve using V-port. *J. Fluids Eng.* **2004**, *126*, 471–481. [\[CrossRef\]](#)
12. Jo, S.H.; Kim, H.J.; Song, K.W. A Numerical Study for Reducing Cavitation in a Butterfly Valve with a Perforated Plate. *Proc. Korean Soc. Fluid Mach.* **2013**, *17*, 65–70. [\[CrossRef\]](#)
13. Lee, M.G.; Lim, C.S.; Han, S.H. Shape design of the bottom plug used in a 3-way reversing valve to minimize the cavitation effect. *Int. J. Precis. Eng. Manuf.* **2016**, *17*, 401–406. [\[CrossRef\]](#)
14. Han, M.X.; Liu, Y.S.; Wu, D.F.; Zhao, X.; Tan, H. A numerical investigation in characteristics of flow force under cavitation state inside the water hydraulic poppet valves. *Int. J. Heat Mass Transf.* **2017**, *111*, 1–16. [\[CrossRef\]](#)
15. Huang, J.T. *Cavitation Principle and Its Application*; Tsinghua University Press: Beijing, China, 1991. (In Chinese)
16. Rasmussen, R.E.H. Some experiments on cavitation erosion in water mixed with air. In Proceedings of the NPL Symposium on Cavitation in Hydrodynamics, London, UK, 1 January 1956.
17. Russell, S.O.; Sheehan, G.J. Effect of entrained air on cavitation erosion. *Can. J. Civ. Eng.* **1974**, *1*, 217–225.
18. Dong, Z.Y. Sonic speed and shock wave in high-velocity aerated flows from high head discharge structures. *J. Hydrodyn. Ser. B* **2003**, *15*, 98–103.
19. Dong, Z.Y.; Su, P.L. Cavitation control by aeration and its compressible characteristics. *J. Hydrodyn. Ser. B* **2006**, *18*, 499–504. [\[CrossRef\]](#)
20. Han, W.; Dong, Z.Y.; Yu, X.W.; Wang, L.; Yan, X.F. High-speed photographic analysis of cavitation characteristics on the condition of aeration. *J. Hydrodyn.* **2010**, *25*, 352–358. [\[CrossRef\]](#)
21. Xu, W.L.; Bai, L.X.; Zhang, F.X. Interaction of a cavitation bubble and an air bubble with a rigid boundary. *J. Hydrodyn.* **2010**, *22*, 503–512. [\[CrossRef\]](#)
22. Luo, J.; Xu, W.L.; Niu, Z.P.; Luo, S.-J.; Zheng, Q.-W. Experimental study of the interaction between the spark-induced cavitation bubble and the air bubble. *J. Hydrodyn.* **2013**, *25*, 859–902. [\[CrossRef\]](#)

23. Guo, Z.P.; Dong, Z.Y.; Han, W. An experimental study on cavitation characteristics of aeration hole with different diameters. *Chin. J. Hydrodyn.* **2013**, *28*, 30–34.
24. Wu, J.H.; Su, K.P.; Wang, Y.; Gou, W. Effect of air bubble size on cavitation erosion reduction. *Sci. China-Techmol. Sci.* **2017**, *60*, 523–528. [[CrossRef](#)]
25. Li, S.; Yang, J.; Ansell, A. Data-driven reduced-order simulation of dam-break flows in a wetted channel with obstacles. *Ocean Eng.* **2023**, *287*, 115826. [[CrossRef](#)]
26. Li, S.; Yang, J.; Liu, W. Estimation of aerator air demand by an embedded multi-gene genetic programming. *J. Hydroinformatics* **2021**, *23*, 1000–1013. [[CrossRef](#)]
27. Tomov, P.; Khelladi, S.; Ravelet, F.; Sarraf, C.; Bakir, F.; Vertenoeuil, P. Experimental study of aerated cavitation in a horizontal venturi nozzle. *Exp. Therm. Fluid Sci.* **2016**, *70*, 85–95. [[CrossRef](#)]
28. Li, R.; Xu, W.L.; Luo, J.; Yuan, H.; Zhao, W.-Y. A Study on Aeration to Alleviate Cavitation Erosion in the Contraction Section of Pressure Flow. *J. Fluids Eng.-Trans. ASME* **2019**, *141*, 091108. [[CrossRef](#)]
29. Koen, J.; Bosman, D.E.; Basson, G.R. Artificial aeration of stepped spillways by crest piers and flares for the mitigation of cavitation damage. *J. S. Afr. Inst. Civ. Eng.* **2019**, *61*, 28–38. [[CrossRef](#)]
30. Abdolapour, M.; Roshan, R. Flow Aeration after Gate in Bottom Outlet Tunnels. *Arab. J. Sci. Eng.* **2014**, *39*, 3441–3448. [[CrossRef](#)]
31. Wang, X.; Hu, Y.A.; Zhang, J.M. Experimental study on anti-cavitation mechanism of valve lintel natural aeration of high head lock. *J. Hydrodyn.* **2019**, *32*, 337–344. [[CrossRef](#)]
32. Li, J.B.; Xu, W.L.; Zhai, Y.W.; Luo, J.; Wu, H.; Deng, J. Influence of multiple air bubbles on the collapse strength of a cavitation bubble. *Exp. Therm. Fluid Sci.* **2020**, *123*, 110328. [[CrossRef](#)]
33. Zhou, S.; Nazari, S.; Hassanzadeh, A.; Bu, X.; Ni, C.; Peng, Y.; Xie, G.; He, Y. The effect of preparation time and aeration rate on the properties of bulk micro-nanobubble water using hydrodynamic cavitation. *Ultrason. Sonochemistry* **2022**, *84*, 105965. [[CrossRef](#)]
34. Salmasi, F.; Abraham, J.; Salmasi, A. Effect of stepped spillways on increasing dissolved oxygen in water, an experimental study. *J. Environ. Manag.* **2021**, *299*, 113600. [[CrossRef](#)] [[PubMed](#)]
35. Wang, J.; Hu, Y.A.; Yan, X.J.; Wu, B.; Zhang, X. Experimental study on hydraulic characteristics of control valve of hydraulic driven ship lift. *J. Yangtze River Chin.* **2021**, *52*, 167–171. [[CrossRef](#)]
36. He, J.; Li, B.; Liu, X. Investigation of flow characteristics in the U-shaped throttle valve. *Adv. Mech. Eng.* **2019**, *11*, 1687814019830492. [[CrossRef](#)]
37. Lu, L.; Zou, J.; Fu, X. The acoustics of cavitation in spool valve with U-notches. *Proc. Inst. Mech. Eng. Part G J. Aerosp. Eng.* **2011**, *226*, 540–549. [[CrossRef](#)]
38. Zhang, C.H.; Lu, F.; Lu, L.Z. High-speed visualization of cavitation evolution around a marine propeller. *J. Vis.* **2019**, *22*, 273–281. [[CrossRef](#)]
39. Xu, W.L.; Wang, Q.F.; Wang, R.W.; Luo, J.; Chen, S.-Y. Effects of air bubble quantity on the reduction of cavitation erosion. *Wear* **2021**, *482–483*, 203937. [[CrossRef](#)]

Disclaimer/Publisher's Note: The statements, opinions and data contained in all publications are solely those of the individual author(s) and contributor(s) and not of MDPI and/or the editor(s). MDPI and/or the editor(s) disclaim responsibility for any injury to people or property resulting from any ideas, methods, instructions or products referred to in the content.